ACS OMEGA

http://pubs.acs.org/journal/acsodf

Article

Quantum Dot-Based Fluorometric Sensor for Hg(II) in Water Customizable for Onsite Visual Detection

Vinayakan Ramachandran Nair,* Madhavan Shanthil, Kulangara Sandeep, Kadencheeri Unnikrishnan Savitha, Aravind Archana, Varghese Deepamol, Chengat Swetha, and Pushpalatha Vijayakumar Vaishag

Cite This: *ACS Omega* 2023, 8, 29468−29474

Read Online

ACCESS | Metrics & More | Article Recommendations | Supporting Information

ABSTRACT: An easy naked-eye detection technique for mercuric ions in water using silanized quantum dots is demonstrated. Cadmium selenide quantum dots were synthesized and rendered water soluble by silica overcoating. The quantum dot emission was instantly turned off by the mercuric ions in the analyte, enabling visual detection. The emission quenching was associated with a concomitant bathochromic shift, both in the absorption and emission profiles. The underlying mechanism is a permanent surface modification of quantum dots by mercuric ions, altering the electronic structure and, in turn, the photophysical properties. The results confirmed the potential of this simple system to be customized for on-site visual detection of mercury contamination in water bodies, biological fluids, and soil with high selectivity and sensitivity.

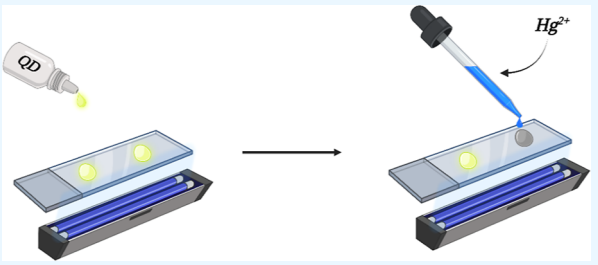

INTRODUCTION

Mercury (Hg) is one of the top ten pollutants listed by the World Health Organization (WHO), as it is a threat to any form of life on earth in either of its variants—elemental mercury, inorganic mercury, or organic mercury.[1−3] Exposure to mercury causes irreversible toxic effects, even in developing fetuses, in the form of neurotoxicity and genotoxicity.[4−6] Through anthropogenic activities over decades, a dangerous hike in mercury concentrations—about 450% above natural levels in the atmosphere—is reported in comparison with the statistics before 1450 AD.[7−9] According to the United Nations' global mercury assessment, the major contributor to freshwater mercury contamination is artisanal and small-scale gold mining industries. When effluents from waste treatment, ore mining, and processing, and the energy sector add to it, the situation becomes more tragic for surface marine waters, the main basement of mercury in the cycle. Here, the organic mercury is accumulated in fish and hence in their consumers, both wildlife and humans.[10−12] Once entered into the body in any of its forms, mercury ends up mainly in the lungs, kidneys, and bloodstream, causing damage to all vital organs and the brain.[13]

Determination of mercury content is challenging due to its high volatility, even at ambient temperatures, and demands sophisticated approaches like gas chromatography,[14] neutron activation analysis,[15] atomic absorption spectroscopy,[16] cold vapor atomic fluorescence spectrometry,[17] cyclic voltammetry,[18] microcantilevers,[19] inductively coupled plasma mass spectrometry,[20] surface-enhanced Raman spectroscopy,[21] microfluidic system,[22] etc. These methods involve multistep sample preparation and/or advanced instrumentation, the hands of trained personnel, and moreover time-consuming experimental procedures. Besides, a compromise between the convenience of on-site testing and its economic viability while relying on these instrumental methods is still a bottleneck. Although many organic fluorophores have been reported with very low detection limits, developing a rapid, cheap, and simple reusable sensor for field detection of mercury ions, especially in water bodies at a ppb level remains a challenge.[23,24] Nanoparticles are proven to be the best building blocks for making low-cost and quick response chemical sensors/chemodosimeters with high specificity for heavy metal ions.[25−32] The detection response is very easy to read out as the signaling transduction is usually via a colorimetric response or an emission switch on/off on interaction with the analyte. The mechanism can be either energy transfer,[33] electron/hole transfer,[34] inner filter effect,[35] agglomeration,[36] ion exchange or complex formation with analytes,[37] etc. Nanoparticles are also ready to go for integration with analytical methods like cyclic voltammetry, surface-enhanced Raman spectroscopy, paper-based colorimetric devices, etc., which makes them more

Received: May 6, 2023
Accepted: July 19, 2023
Published: August 2, 2023

https://doi.org/10.1021/acsomega.3c03125
ACS Omega 2023, 8, 29468−29474

acceptable compared to organic fluorophores in designing sensors with high specificity and a low detection limit.[38−42] Although a variety of nanomaterials are studied and reported, quantum dots stand alone due to their unique characteristics such as sharp emission with high quantum yield, robustness, and stability, which are the most desirable properties for a signaling center.[43−50]

In the present study, we demonstrate a naked eye, rapid, and selective detection of mercuric ions in water using the QD emission "switch-off" strategy. To the best of our knowledge, this is the first demonstration of mercuric ion sensing in water using silanized cadmium selenide (CdSe) QDs. Hitherto, many groups have successfully come up with mercury detecting systems based on quantum dots, with detection limits down to nanomolar. Most of them are designed via surface modification with suitable molecules like proteins,[51] nucleotides,[52] DNA,[53] polymers,[54] amino acids,[55] etc., which are often labor- and cost-intensive as well as time consuming. In this work, we have used a label-free detection probe where no surface modification or functionalization protocols are necessary. More importantly, the presence of mercuric ions, even in the presence of other interfering ions, can be viewed just by mixing QDs and water samples on a glass slide and illuminating under a UV lamp.

RESULTS AND DISCUSSION

Water-soluble, luminescent silanized cadmium selenide quantum dots (QDs) were prepared by following a reverse microemulsion method as described elsewhere.[56,57] QDs used in the present study showed the first excitonic absorption peak at ∼575 nm and the emission maximum centered at 582 nm (blue trace in Figures 1A and 2A) in phosphate buffered saline

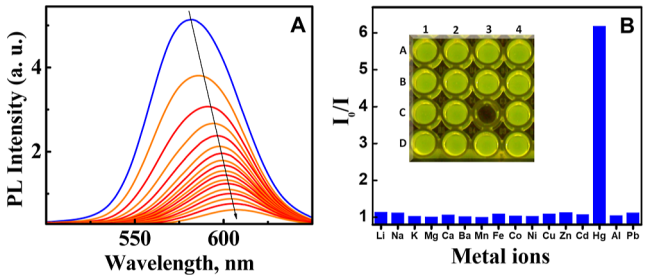

Figure 1. (A) Emission spectra of silanized CdSe QDs (0.16 μM, PBS, pH 7.3) in the presence of mercuric ions (0−14 μM). (B) Selectivity of Hg^{2+} compared to other cations (∼100 μM). Inset photograph showing visual detection under a UV lamp: A_1-Li^+, A_2-Na^+, A_3-K^+, A_4-Mg^{2+}, B_1-Ca^{2+}, B_2-Ba^{2+}, B_3-Mn^{2+}, B_4-Fe^{2+}, C_1-Co^{2+}, C_2-Ni^{2+}, C_3-Hg^{2+}, C_4-Cu^{2+}, D_1-Zn^{2+}, D_2-Cd^{2+}, D_3-Al^{3+}, and D_4-Pb^{2+}.

(PBS). The stability of QDs under various pH conditions and the ionic strength of the medium were examined systematically and showed excellent shelf life, even for months in the suspension phase. The details of characterization and stability studies are provided in the Supporting Information.

Experiments were conducted by adding aqueous solutions of metal ion salts into a silanized QD suspension (0.16 μm in PBS buffer pH 7.3) and monitoring absorption and emission spectral properties systematically as a function of cation concentration. We observed an instantaneous and stepwise decrease in the emission intensity of QDs with an increase in the concentration of mercuric ions (Figure 1A). The emission was completely shut off at ∼14 μM loading of mercuric ions.

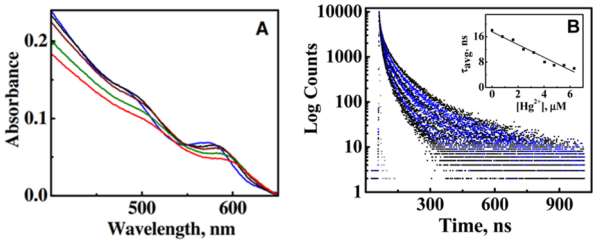

Figure 2. (A) Absorption spectra of silanized CdSe QDs (0.16 μM, PBS, pH 7.3), in presence of Hg^{2+} (0−14 μM), excited at 480 nm. (B) Corresponding change in exciton decay lifetimes. Excited at 441 nm. Inset confirms a considerable decrease in the average exciton lifetime on interaction with mercuric ions.

Surprisingly, this permanent shut off in QD emission was so specific to mercuric ions as the other common metal ions like Li^+, Na^+, K^+, Mg^{2+}, Ca^{2+}, Ba^{2+}, Mn^{2+}, Fe^{2+}, Co^{2+}, Ni^{2+}, Cu^{2+}, Zn^{2+}, Cd^{2+}, Al^{3+}, and Pb^{2+} left an unaltered emission intensity even at a very high loading of about 100 μM (Figure 1B).

It is quite noticeable that both the absorption and emission profiles were affected while interacting with mercuric ions (Figures 1A and 2A). Emission intensity was instantly and permanently "turned off", with a concomitant spectral broadening on successive additions of mercuric ions. More importantly, both absorption and emission maxima showed a gradual red shift, to an extent of 25 nm, while adding analytes up to 14 μM, where the emission was completely quenched. The bathochromic shift in the absorption spectrum accommodated a mere shift in excitonic positions, keeping the overall features intact. Furthermore, to probe the mode of interaction between the analyte and QD, the exciton lifetime of QD was measured as a function of analyte concentration (Figure 2B). QDs showed a triexponential exciton decay characteristics with an average lifetime of 18 ns, which was remarkably reduced to 7 ns (∼70% loss) in the presence of mercuric ions (Table S1). Changes in absorption excitonic position along with a considerable change in exciton decay lifetime indicated a ground state interaction of mercuric ions with QDs, which modified the electronic band structure.

It is possible to account for the redshift in the excitonic transition in the absorption spectrum of QDs in terms of (i) an increase in the overall size of the QDs due to Ostwald's ripening[58] or (ii) a metal ion-induced aggregation of QDs.[59,60] These possibilities can also result in emission quenching and spectral broadening as the QD electronic energy levels are influenced in either case. A high-resolution electron microscopic (HRTEM) study in the absence and presence of mercuric ions was done to resolve these assumptions (Figure 3). HRTEM images showed that the average size of QD as well as its distribution remained unaffected in presence of mercuric ions. It rules out any chance of an increase in QD size and/or metal ion induced aggregation. Further, any turbidity on introducing mercuric ions, even at higher concentrations was not observed for QD suspension, which could be observable if a metal ion induced aggregation was prevalent. Also, a possibility of hole scavenging is ruled out, since mercuric ions cannot be easily oxidized.

The QD emission quenching along with a bathochromic shift in QD absorption and emission maxima in the presence of mercuric ions can be explained based on the interaction of metal ions with QDs, leading to the generation of new trap states with low-lying energy levels. The bathochromic shift in

https://doi.org/10.1021/acsomega.3c03125
ACS Omega 2023, 8, 29468−29474

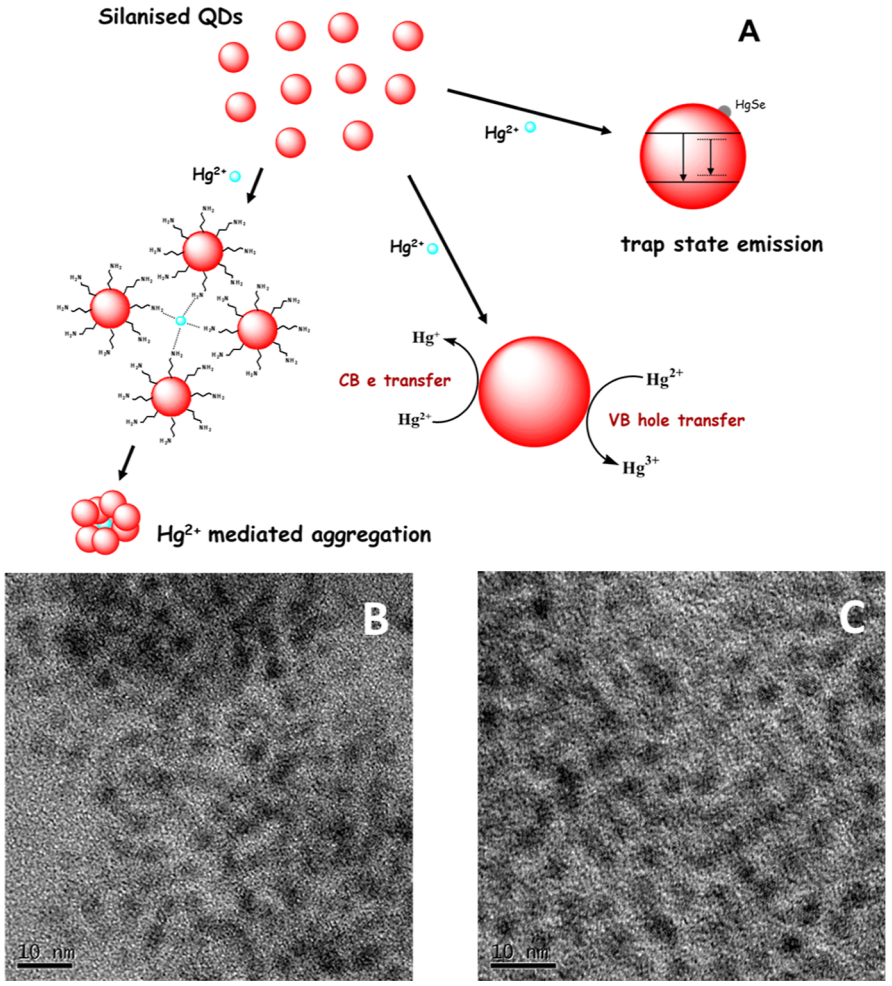

Figure 3. (A) Schematic representation of various possibilities that leads to emission quenching of QDs, while interacting with Hg^{2+} ions. HRTEM images of silanized QDs: (B) in absence of mercuric ions. (C) After adding Hg^{2+}. Neither an increase in size or aggregation is observed.

the first excitonic position of the QD absorption spectrum on adding mercuric ions (Figure 2A), corresponds to a reduction in the energy gap of QDs from 2.16 to 2.07 eV. This can be attributed to the generation of new energy levels close to the valence and conduction band edges. Weller and co-workers have earlier reported a red shift in the excitonic absorption peak and a reduction in band edge emission intensity in the case of cadmium sulfide (CdS) QDs on the addition of mercuric ions. This is ascribed to the formation of quantum sized HgS on the CdS surface, which alters the electronic structure of QDs by generating new nonradiative decay channels having lower energy states.[61−63] Similar surface modifications in the case of cadmium telluride (CdTe) QDs were reported by Rogach and co-workers, where mercuric ions react with the QD surface, leading to the formation of quantum sized HgTe.[64] Extending the same chemistry to the present observation, mercuric ions are expected to react with the CdSe QDs surface, leading to the formation of quantum-sized HgSe on the QD surface, opening a new low energy nonradiative channel for exciton decay.

$$(CdSe)n + Hg^{2+} \rightarrow Cd_{n-1}HgSe_n + Cd^{2+}$$

The red shift in absorption and emission maxima and concomitant broadening of the emission profile can be thus attributed to the formation of HgSe on the QD surface. It is also supported by the fact that the solubility product of HgSe ($-\log K_{sp} = 65$) is lower compared to that of CdSe ($-\log K_{sp} = 35$).[65]

In the absence of HgSe formation, the excitons formed in CdSe QDs underwent the usual radiative recombination. Mercuric ions modified the QD surface and altered the electronic structure, which resulted in (i) a smaller band gap, as evident from the considerable redshift in the excitonic absorption peaks and emission maximum and (ii) crystal defects like shallow and deep trap states, which broadened the emission spectrum. This assumption is well supported by a substantial reduction in the average lifetime, from 22 to 7 ns, in the presence of mercuric ions, due to the opening of new depopulation channels in the form of defects (Figure 4).

Obviously, the cation exchange reaction is plausible only if the mercuric ions directly interact with the QD surface, crossing the siloxane shell. HRTEM images showed the presence of a very thin siloxane shell (~1.5 nm, Figure 5C) formed by hydrolysis and condensation of aminopropyl silane (APS). The structural backbone of silica shell is a three-dimensional network of a dimer formed by APS through a siloxane bond, with one amino group anchoring on the QD surface while the other one projecting toward the periphery. From a simple ball and stick model, the overall length of this dimer is approximately estimated as 1.5 nm (Figure 5D). Moreover, the porosity of the siloxane shell is enough to facilitate the pass through of mercuric ions, as reported in the

https://doi.org/10.1021/acsomega.3c03125
ACS Omega 2023, 8, 29468−29474

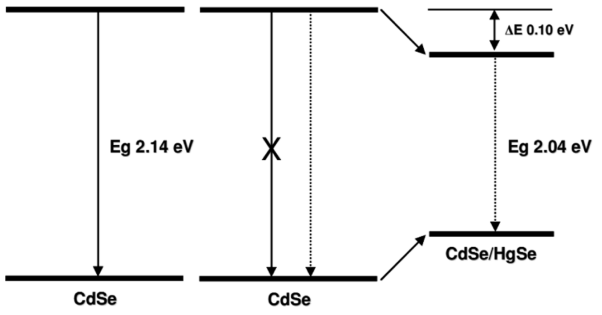

Figure 4. Exciton recombination pathways in CdSe QDs (solid arrow) and in the presence of HgSe on the CdSe QD surface (dashed arrow). The ΔE corresponds to the redshift in the excitonic peak of about 25 nm.

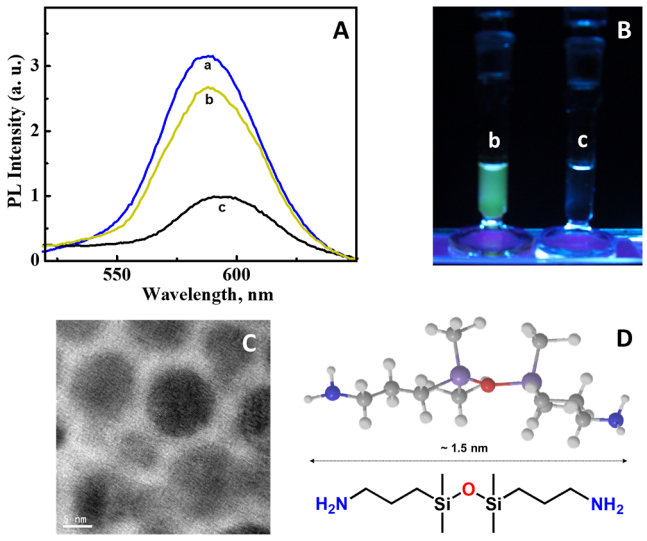

Figure 5. (A) QD emission: a → in the absence of any analytes, b → in a pool of 15 metal ions used in this study, and c → b + Hg^{2+}. (B) Photograph of b and c. (C) HRTEM showing a thin silica shell over the QD core. (D) Overall length of an APS dimer on the QD surface obtained from the minimum energy optimized structure using Chem3D.

case of silica over coated CdS QDs studied by Iwasaki et al.[66−68]

The specificity of the QD probe toward mercuric ions was further confirmed by conducting emission quenching studies in the presence of other probable metal ions in water. QD dispersion was initially loaded with a very high amount of metal ion salts (Li^+, Na^+, K^+, Mg^{2+}, Ca^{2+}, Ba^{2+}, Mn^{2+}, Fe^{2+}, Co^{2+}, Ni^{2+}, Cu^{2+}, Zn^{2+}, Cd^{2+}, Al^{3+}, Pb^{2+}; ∼90 μM each). The decrease in the emission intensity was found to be negligible (∼10%; trace "b" in Figure 5A). But the addition of mercuric ions (8 μM) to this QD—metal ions pool resulted in a substantial reduction in the luminescence intensity of QDs (trace "c" in Figure 5A). It clearly indicated the possibility of using QDs for the selective detection of mercuric ion contamination in raw water, without the aid of any sophisticated instruments but with a handheld UV lamp (Figure 5B and the video link provided in the Supporting Information). The corresponding limit of detection (LOD) was estimated as 1.5 ppm (according to the 3σ IUPAC definition).[69]

CONCLUSIONS

We have demonstrated the use of QDs in the selective detection of mercuric ions in water by an instant emission switch off, even in the presence of interfering metal ions, with a LOD down to 1.5 ppm. The photophysical properties of QDs were dramatically influenced by mercuric ions: a bathochromic shift in the absorption and emission spectra along with a decrease in the luminescence intensity were observed. It is anticipated that the mesoporous, thin silica shell is permeable to mercuric ions, allowing interaction with the CdSe core surface. The spectral changes are attributed to the formation of quantum-sized HgSe on the CdSe surface. In short, silanized QDs open up an easy fluorometric method for the naked eye detection of mercuric ions in the presence of other interfering metal ions, without the aid of any specialized instruments. This straightforward technique is customizable for the on-site analysis of real samples from water bodies, biological systems, and soil to visually identify mercuric ions without cross-sensitivities, simply with the help of a hand-held UV lamp.

MATERIALS AND METHODS

The electronic absorption spectra were recorded on a Shimadzu Model UV-3101 or a 2401 PC UV−vis−NIR scanning spectrophotometer; emission spectra were collected using a SPEX-Fluorolog F112X spectrofluorimeter, and photoluminescence lifetimes were measured using an IBH Picosecond single photon counting system with an excitation source of 440 nm (pulse width <200 ps), and luminescence decay profiles were deconvoluted using IBH data station software V2.1. Fourier transform infrared (FTIR) studies were performed using a Shimadzu IR Prestige-21 FTIR spectrometer. X-ray diffraction patterns were recorded using the Philips X'Pert Pro, X-ray diffractometer with Cu Kα radiation (1.5406 Å) and spectra were analyzed using X'Pert Highscore software. For HRTEM studies, a drop of nanoparticle solution was placed on a carbon-coated Cu grid, and the solvent was allowed to evaporate. Specimens were imaged on a FEI Tecnai G^2 S-TWIN 300 kV high-resolution transmission electron microscope. Melting points were determined on a Mel-Temp II melting point apparatus.

All the spectroscopic studies were carried out at ambient and identical conditions (unless specified) where the QD concentration was in a micro molar (∼0.17 μM) range and PL spectra were collected by exciting at 450 nm (OD ≈ 0.05) for all samples. Also, we have accounted for the small dilution effect (<2%) by performing control experiments. Experiments were performed using spectroscopic grade solvents, double distilled/deionized water, and PBS (pH 7.3). Reagents used were purchased from Aldrich, Merck, and Fluka and used as such.

EXPERIMENTAL SECTION

Synthesis of TOPO-Capped CdSe QDs. A reaction mixture containing cadmium oxide (0.067 g, 0.52 mM), dodecylamine (3.8 g, 20.7 mM), trioctylphosphine oxide (2.7 g, 6.9 mM), and tetradecylphosphonic acid (0.40 g, 1.4 mM) was heated to 300 °C until cadmium oxide dissolved completely to produce an optically clear solution. Keeping the temperature at 300 °C, an injection mixture containing TOPSe (83 μL, 0.08 mM) and TOP (5.2 mL, 2.5 mM) was introduced. After the desired crystal growth, the reaction was arrested by reducing the reaction temperature to ambient

https://doi.org/10.1021/acsomega.3c03125
ACS Omega 2023, 8, 29468−29474

conditions, and the QDs thus obtained were purified by size selective precipitation using methanol, followed by centrifugation. QDs were characterized by spectroscopic and HRTEM analyses and their average size was estimated as 7.3 nm.

Synthesis of Silica-Overcoated CdSe QDs. Cyclohexane (10 mL) was added with a mixture of Igepal CO-520 (1.3 mL), CdSe QDs (400 μL) along with APS (63 μL, 0.36 mM) and stirred vigorously for 30 min under inert atmosphere. Then, ammonia solution (150 μL, 33 wt %) was added, and the stirring was continued for 24 h. The salinized QDs were precipitated as globules, which was further purified by washing with dry chloroform (4 mL) five times to remove unreacted components and then redissolved in PBS (pH 7.3). Igepal CO-520 (1.3 mL) was dissolved in cyclohexane (10 mL) by stirring under an inert atmosphere for 30 min.

■ ASSOCIATED CONTENT

Supporting Information

The Supporting Information is available free of charge at https://pubs.acs.org/doi/10.1021/acsomega.3c03125.

Characterization of quantum dots, stability of QDs under various pH and ionic strength of the medium, shelf-life, and lifetime analysis (PDF)

■ AUTHOR INFORMATION

Corresponding Author

Vinayakan Ramachandran Nair − *Department of Chemistry (Research Center under MG University, Kerala), NSS Hindu College (Nationally Accredited with "A" Grade), Changanacherry 686102 Kerala, India; Chemical Sciences and Technology Division, National Institute for Interdisciplinary Science and Technology (NIIST-CSIR), Thiruvananthapuram 695019 Kerala, India;* orcid.org/0000-0003-0082-3659; Email: rvinayakan@gmail.com

Authors

Madhavan Shanthil − *Department of Chemistry, Government Victoria College, Research Center under University of Calicut, Palakkad 678001 Kerala, India;* orcid.org/0000-0002-6478-1155

Kulangara Sandeep − *Department of Chemistry, Government Victoria College, Research Center under University of Calicut, Palakkad 678001 Kerala, India;* orcid.org/0000-0002-4275-3495

Kadencheeri Unnikrishnan Savitha − *Department of Chemistry (Research Center under MG University, Kerala), NSS Hindu College (Nationally Accredited with "A" Grade), Changanacherry 686102 Kerala, India*

Aravind Archana − *Aravind Archana—Saveetha School of Engineering SIMATS, Chennai 602105 Tamilnadu, India;* orcid.org/0000-0002-3718-0063

Varghese Deepamol − *PG Department of Chemistry, Alphonsa College, Pala 686 574 Kerala, India*

Chengat Swetha − *Department of Chemistry, St. Thomas College, Ranni 689673 Kerala, India*

Pushpalatha Vijayakumar Vaishag − *Department of Chemistry, Government Victoria College, Research Center under University of Calicut, Palakkad 678001 Kerala, India*

Complete contact information is available at: https://pubs.acs.org/10.1021/acsomega.3c03125

Notes

The authors declare no competing financial interest.

■ ACKNOWLEDGMENTS

V.R., K.S., and M.S. sincerely acknowledge the mentorship, guidance, and limitless support from Professor (Dr.) K. George Thomas, Dean (Faculty Affairs), School of Chemistry, IISER Trivandrum, India, for the completion of this work. The authors thank Robert Philip, senior technical assistant, NIIST-CSIR, for helping with HRTEM studies.

■ REFERENCES

(1) Driscoll, C. T.; Mason, R. P.; Chan, H. M.; Jacob, D. J.; Pirrone, N. Mercury as a Global Pollutant: Sources, Pathways, and Effects. *Environ. Sci. Technol.* **2013**, *47*, 4967−4983.

(2) Feng, X.; Li, P.; Fu, X.; Wang, X.; Zhang, H.; Lin, C. J. Mercury pollution in China: implications on the implementation of the Minamata Convention. *Environ. Sci.: Processes Impacts.* **2022**, *24*, 634−648.

(3) Outridge, P. M.; Mason, R. P.; Wang, F.; Guerrero, S.; Heimbürger-Boavida, L. E. Updated global and oceanic mercury budgets for the United Nations global mercury assessment. *Environ. Sci. Technol.* **2018**, *52*, 11466−11477.

(4) Cheung, M. K.; Verity, M. A. Experimental methyl mercury neurotoxicity: locus of mercurial inhibition of brain protein synthesis *in vivo* and *in vitro*. *J. Neurochem.* **1985**, *44*, 1799−1808.

(5) Tchounwou, P. B.; Ayensu, W. K.; Ninashvili, N.; Sutton, D. Review: Environmental exposure to mercury and its toxicopathologic implications for public health. *Environ. Toxicol.* **2003**, *18*, 149−175.

(6) Teitelbaum, C. S.; Ackerman, J. T.; Hill, M. A.; Satter, J. M.; Casazza, M. L.; De La Cruz, S. E. W.; Boyce, W. M.; Buck, E. J.; Eadie, J. M.; Herzog, M. P.; Matchett, E. L.; Overton, C. T.; Peterson, S. H.; Plancarte, M.; Ramey, A. M.; Sullivan, J. D.; Prosser, D. J. Avian influenza antibody prevalence increases with mercury contamination in wild waterfowl. *Proc. R. Soc. B.* **2022**, *289*, 20221312.

(7) UN Environment. *Global Mercury Assessment 2018. UN Environment Programme*; Chemicals and Health Branch: Geneva, Switzerland, 2019; ISBN: 978-92-807-3744-8.

(8) Streets, D. G.; Horowitz, H. M.; Jacob, D. J.; Lu, Z.; Levin, L.; ter Schure, A. F. H.; Sunderland, E. M. Tootal mercury released to the environment by human activities. *Environ. Sci. Technol.* **2017**, *51*, 5969−5977.

(9) Obrist, D.; Kirk, J. L.; Zhang, L.; Sunderland, E. M.; Jiskra, M.; Selin, N. E. A review of global environmental mercury processes in response to human and natural perturbations: Changes of emissions, climate, and land use. *Ambio* **2018**, *47*, 116−140.

(10) Miraly, H.; Razavi, N. R.; Vogl, A. A.; Kraus, R. T.; Gorman, A. M.; Limburg, K. E. Tracking fish lifetime exposure to mercury using eye lenses. *Environ. Sci. Technol. Lett.* **2023**, *10*, 222−227.

(11) Fitzgerald, W. F.; Lamborg, C. H.; Hammerschmidt, C. R. Marine biogeochemical cycling of mercury. *Chem. Rev.* **2007**, *38*, 641−662.

(12) Zalups, R. K. Molecular interactions with mercury in the kidney. *Pharmacol. Rev.* **2000**, *52*, 113−144.

(13) Järup, L. Hazards of heavy metal contamination. *Br. Med. Bull.* **2003**, *68*, 167−182.

(14) Gras, R.; Luong, J.; Shellie, R. A. Direct measurement of trace elemental mercury in hydrocarbon matrices by gas chromatography with ultraviolet photometric detection. *Anal. Chem.* **2015**, *87*, 11429−11432.

(15) Buenafama, H. D.; Lubkowitz, J. A. Analysis of organically bound mercury via neutron activation analysis. *J. Radioanal. Nucl. Chem.* **1975**, *25*, 239−246.

(16) Lei, Y.; Zhang, F.; Guan, P.; Guo, P.; Wang, G. Rapid and selective detection of Hg(II) in water using Au NP in situ-modified filter paper by a head-space solid phase extraction Zeeman atomic absorption spectroscopy method. *New J. Chem.* **2020**, *44*, 14299−14305.

(17) Ebdon, L.; Foulkes, M. E.; Le Roux, S.; Muñoz-Olivas, R. Cold vapour atomic fluorescence spectrometry and gas chromatography-pyrolysis-atomic fluorescence spectrometry for routine determination of total and organometallic mercury in food samples. *Analyst* **2002**, *127*, 1108−1114.
(18) Tercier-Waeber, M.-L.; Abdou, M.; Fighera, M.; Kowal, J.; Bakker, E.; van der Wal, P. In situ voltammetric sensor of potentially bioavailable inorganic mercury in marine aquatic systems based on gel-integrated nanostructured gold-based microelectrode arrays. *ACS Sens.* **2021**, *6*, 925−937.
(19) Thundat, T.; Wachter, E. A.; Sharp, S. L.; Warmack, R. J. Detection of mercury vapor using resonating microcantilevers. *Appl. Phys. Lett.* **1995**, *66*, 1695−1697.
(20) Tao, H.; Murakami, T.; Tominaga, M.; Miyazaki, A. Mercury speciation in natural gas condensate by gas chromatography-inductively coupled plasma mass spectrometry. *J. Anal. At. Spectrom.* **1998**, *13*, 1085−1093.
(21) Sarfo, D. K.; Sivanesan, A.; Izake, E. L.; Ayoko, G. A. Rapid detection of mercury contamination in water by surface enhanced Raman spectroscopy. *RSC Adv.* **2017**, *7*, 21567−21575.
(22) Bell, J.; Climent, E.; Hecht, M.; Buurman, M.; Rurack, K. Combining a droplet-based microfluidic tubing system with gated indicator releasing nanoparticles for mercury trace detection. *ACS Sens.* **2016**, *1*, 334−338.
(23) Chen, Y.; Zhang, W.; Cai, Y.; Kwok, R. T. K.; Hu, Y.; Lam, J. W. Y.; Gu, X.; He, Z.; Zhao, Z.; Zheng, X.; Chen, B.; Gui, C.; Tang, B. Z. AIEgens for dark through-bond energy transfer: design, synthesis, theoretical study and application in ratiometric Hg^{2+} sensing. *Chem. Sci.* **2017**, *8*, 2047−2055.
(24) Wu, S.; Yang, Y.; Cheng, Y.; Wang, S.; Zhou, Z.; Zhang, P.; Zhu, X.; Wang, B.; Zhang, H.; Xie, S.; Zeng, Z.; Tang, B. Z. Fluorogenic detection of mercury ion in aqueous environment using hydrogel-based Aie sensing films. *Aggregate* **2022**, *4*, No. e287.
(25) Li, Y.; Xie, J.-F.; Chang, C.-C.; Wang, C.-M.; Tu, H.-L. Highly sensitive detection of mercury ions using zincophosphite framework nanoparticle−polyaniline composites. *ACS Appl. Nano Mater.* **2020**, *3*, 9724−9730.
(26) Mariyappan, V.; Manavalan, S.; Chen, S.-M.; Jaysiva, G.; Veerakumar, P.; Keerthi, M. Sr@FeNi-S Nanoparticle/carbon nanotube nanocomposite with superior electrocatalytic activity for electrochemical detection of toxic mercury(II). *ACS Appl. Electron. Mater.* **2020**, *2*, 1943−1952.
(27) Escandar, G. M.; Olivieri, A. C. A critical review on the development of optical sensors for the determination of heavy metals in water samples. the case of mercury(II) ion. *ACS Omega* **2022**, *7*, 39574−39585.
(28) Schiesaro, I.; Burratti, L.; Meneghini, C.; Fratoddi, I.; Prosposito, P.; Lim, J.; Scheu, C.; Venditti, I.; Iucci, G.; Battocchio, C. Hydrophilic silver nanoparticles for Hg(II) detection in water: direct evidence for mercury−silver interaction. *J. Phys. Chem. C* **2020**, *124*, 25975−25983.
(29) Chen, G.; Guo, Z.; Zeng, G.; Tang, L. Fluorescent and colorimetric sensors for environmental mercury detection. *Analyst* **2015**, *140*, 5400−5443.
(30) Montes-García, V.; Squillaci, M. A.; Diez-Castellnou, M.; Ong, Q. K.; Stellacci, F.; Samorì, P. Chemical sensing with Au and Ag nanoparticles. *Chem. Soc. Rev.* **2021**, *50*, 1269−1304.
(31) Dai, D.; Yang, J.; Wang, Y.; Yang, Y.-W. Recent progress in functional materials for selective detection and removal of mercury-(II) ions. *Adv. Funct. Mater.* **2021**, *31*, 2006168.
(32) Govindaraju, S.; Puthiaraj, P.; Lee, M.-H.; Yun, K. Photoluminescent AuNCs@UiO-66 for ultrasensitive detection of mercury in water samples. *ACS Omega* **2018**, *3*, 12052−12059.
(33) Liu, B.; Zeng, F.; Wu, G.; Wu, S. Nanoparticles as scaffolds for FRET-based ratiometric detection of mercury ions in water with QDs as donors. *Analyst* **2012**, *137*, 3717−3724.
(34) Tan, H.; Liu, B.; Chen, Y. Lanthanide coordination polymer nanoparticles for sensing of mercury(II) by photoinduced electron transfer. *ACS Nano* **2012**, *6*, 10505−10511.
(35) Gu, W.; Pei, X.; Cheng, Y.; Zhang, C.; Zhang, J.; Yan, Y.; Ding, C.; Xian, Y. Black phosphorus quantum dots as the ratiometric fluorescence probe for trace mercury ion detection based on inner filter effect. *ACS Sens.* **2017**, *2*, 576−582.
(36) Adsetts, J. R.; Hoesterey, S.; Gao, C.; Love, D. A.; Ding, Z. Electrochemiluminescence and photoluminescence of carbon quantum dots controlled by aggregation-induced emission, aggregation-caused quenching, and interfacial reactions. *Langmuir* **2020**, *36*, 14432−14442.
(37) Huang, D.; Niu, C.; Ruan, M.; Wang, X.; Zeng, G.; Deng, C. Highly sensitive strategy for Hg^{2+} detection in environmental water samples using long lifetime fluorescence quantum dots and gold nanoparticles. *Environ. Sci. Technol.* **2013**, *47*, 4392−4398.
(38) Zhou, G.; Chang, J.; Pu, H.; Shi, K.; Mao, S.; Sui, X.; Ren, R.; Cui, S.; Chen, J. Ultrasensitive mercury ion detection using DNA-functionalized molybdenum disulfide nanosheet/gold nanoparticle hybrid field-effect transistor device. *ACS Sens.* **2016**, *1*, 295−302.
(39) Chung, E.; Gao, R.; Ko, J.; Choi, N.; Lim, D. W.; Lee, E. K.; Chang, S. I.; Choo, J. Trace analysis of mercury(II) ions using aptamer-modified Au/Ag core−shell nanoparticles and SERS spectroscopy in a microdroplet channel. *Lab Chip* **2013**, *13*, 260−266.
(40) Chen, G.-H.; Chen, W.-Y.; Yen, Y.-C.; Wang, C.-W.; Chang, H.-T.; Chen, C.-F. Detection of mercury(II) ions using colorimetric gold nanoparticles on paper-based analytical devices. *Anal. Chem.* **2014**, *86*, 6843−6849.
(41) Chen, W.; Fang, X.; Li, H.; Cao, H.; Kong, J. A simple paper-based colorimetric device for rapid mercury(II) assay. *Sci. Rep.* **2016**, *6*, 31948.
(42) Gréboval, C.; Chu, A.; Goubet, N.; Livache, C.; Ithurria, S.; Lhuillier, E. Mercury chalcogenide quantum dots: material perspective for device integration. *Chem. Rev.* **2021**, *121*, 3627−3700.
(43) Gu, S.; Hsieh, C.-T.; Tsai, Y.-Y.; Ashraf Gandomi, Y.; Yeom, S.; Kihm, K. D.; Fu, C.-C.; Juang, R.-S. Sulfur and nitrogen co-doped graphene quantum dots as a fluorescent quenching probe for highly sensitive detection toward mercury ions. *ACS Appl. Nano Mater.* **2019**, *2*, 790−798.
(44) Das, S.; Rakshit, S.; Datta, A. Mechanistic insights into selective sensing of Pb^{2+} in water by photoluminescent CdS quantum dots. *J. Phys. Chem. C* **2021**, *125*, 15396−15404.
(45) Patir, K.; Gogoi, S. K. Facile synthesis of photoluminescent graphitic carbon nitride quantum dots for Hg^{2+} detection and room temperature phosphorescence. *ACS Sustainable Chem. Eng.* **2018**, *6*, 1732−1743.
(46) Reagen, S.; Wu, Y.; Liu, X.; Shahni, R.; Bogenschuetz, J.; Wu, X.; Chu, Q. R.; Oncel, N.; Zhang, J.; Hou, X.; Combs, C.; Vasquez, A.; Zhao, J. X. Synthesis of highly near-infrared fluorescent graphene quantum dots using biomass-derived materials for in vitro cell imaging and metal ion detection. *ACS Appl. Mater. Interfaces* **2021**, *13*, 43952−43962.
(47) Liang, S.; Chen, J.; Pierce, D. T.; Zhao, J. X. A turn-on fluorescent nanoprobe for selective determination of selenium(IV). *ACS Appl. Mater. Interfaces* **2013**, *5*, 5165−5173.
(48) Nair, A. N.; Chava, V. S.; Bose, S.; Zheng, T.; Pilla, S.; et al. In situ doping-enabled metal and nonmetal codoping in graphene quantum dots: synthesis and application for contaminant sensing. *ACS Sustainable Chem. Eng.* **2020**, *8*, 16565−16576.
(49) Singh, S.; Vaishnav, J. K.; Mukherjee, T. K. Quantum dot-based hybrid coacervate nanodroplets for ultrasensitive detection of Hg^{2+}. *ACS Appl. Nano Mater.* **2020**, *3*, 3604−3612.
(50) Subramaniyan, S. B.; Veerappan, A. Water soluble cadmium selenide quantum dots for ultrasensitive detection of organic, inorganic and elemental mercury in biological fluids and live cells. *RSC Adv.* **2019**, *9*, 22274−22281.
(51) Paramanik, B.; Bhattacharyya, S.; Patra, A. Detection of Hg^{2+} and F^- ions by using fluorescence switching of quantum dots in an au-cluster−CdTe QD nanocomposite. *Chem.—Eur. J.* **2013**, *19*, 5980−5987.
(52) Liu, M.; Wang, Z.; Zong, S.; Chen, H.; Zhu, D.; Wu, L.; Hu, G.; Cui, Y. SERS detection and removal of mercury(II)/silver(I) using

https://doi.org/10.1021/acsomega.3c03125
ACS Omega 2023, 8, 29468−29474

oligonucleotide-functionalized core/shell magnetic silica sphere@Au nanoparticles. *ACS Appl. Mater. Interfaces* **2014**, *6*, 7371−7379.
(53) Srinivasan, K.; Subramanian, K.; Murugan, K.; Dinakaran, K. Sensitive fluorescence detection of mercury(II) in aqueous solution by the fluorescence quenching effect of MoS_2 with DNA functionalized carbon dots. *Analyst* **2016**, *141*, 6344−6352.
(54) Aziz, K. H. H.; Omer, K. M.; Hamarawf, R. F. Lowering the detection limit towards nanomolar mercury ion detection via surface modification of N-doped carbon quantum dots. *New J. Chem.* **2019**, *43*, 8677−8683.
(55) Du, W.; Liao, L.; Yang, L.; et al. Aqueous synthesis of functionalized copper sulfde quantum dots as near-infrared luminescent probes for detection of Hg^{2+}, Ag^{+} and Au^{3+}. *Sci. Rep.* **2017**, *7*, 11451.
(56) Vibin, M.; Vinayakan, R.; John, A.; Raji, V.; Rejiya, C. S.; Vinesh, N. S.; Abraham, A. Cytotoxicity and fluorescence studies of silica-coated CdSe quantum dots for bioimaging applications. *J. Nanopart. Res.* **2011**, *13*, 2587−2596.
(57) Vinayakan, R.; Shanmugapriya, T.; Nair, P. V.; Ramamurthy, P.; Thomas, K. G. An approach for optimizing the shell thickness of core−shell quantum dots using photoinduced charge transfer. *J. Phys. Chem. C* **2007**, *111*, 10146−10149.
(58) Tonti, D.; Mohammed, M. B.; Al-Salman, A.; Pattison, P.; Chergui, M. Multimodal distribution of quantum confinement in ripened CdSe nanocrystals. *Chem. Mater.* **2008**, *20*, 1331−1339.
(59) Koole, R.; Liljeroth, P.; de Mello Donegá, C.; Vanmaekelbergh, D.; Meijerink, A. Electronic coupling and exciton energy transfer in CdTe quantum-dot molecules. *J. Am. Chem. Soc.* **2006**, *128*, 10436−10441.
(60) Ke, J.; Li, X.; Zhao, Q.; Hou, Y.; Chen, J. Ultrasensitive quantum dot fluorescence quenching assay for selective detection of mercury ions in drinking water. *J. Sci. Rep.* **2014**, *4*, 5624.
(61) Eychmüller, A.; Hässelbarth, A.; Weller, H. J. Quantum-sized HgS in contact with quantum-sized CdS colloids. *J. Lumin.* **1992**, *53*, 113−115.
(62) Haesselbarth, A.; Eychmueller, A.; Eichberger, R.; Giersig, M.; Mews, A.; et al. Chemistry and photophysics of mixed cadmium sulfide/mercury sulfide colloids. *J. Phys. Chem.* **1993**, *97*, 5333−5340.
(63) Eychmüller, A. Structure and photophysics of semiconductor nanocrystals. *J. Phys. Chem. B* **2000**, *104*, 6514−6528.
(64) Susha, A. S.; Javier, A. M.; Parak, W. J.; et al. Luminescent CdTe nanocrystals as ion probes and pH sensors in aqueous solutions. *Colloids Surf., A* **2006**, *281*, 40−43.
(65) Szabo, J. P.; Cocivera, M. Mechanism of electrodeposition of cadmium selenide from $SeSO_3^{2-}$ solution. *Can. J. Chem.* **1988**, *66*, 1065−1072.
(66) Iwasaki, K.; Torimoto, T.; Shibayama, T.; Takahashi, H.; Ohtani, B. Preparation and characterization of water-soluble jingle-bell-shaped silica-coated cadmium sulfide nanoparticles. *J. Phys. Chem. B* **2004**, *108*, 11946−11952.
(67) Suryanarayanan, V.; Nair, A. S.; Tom, R. T.; et al. Porosity of core−shell nanoparticles. *J. Mater. Chem.* **2004**, *14*, 2661−2666.
(68) Iwasaki, K.; Torimoto, T.; Shibayama, T.; Nishikawa, T.; Ohtani, B. Fabrication of jingle-bell-shaped core−shell nanoparticulate films and molecular-size-responsive photoluminescence quenching of cadmium sulfide cores. *Small* **2006**, *2*, 854−858.
(69) Ostra, M.; Ubide, C.; Vidal, M.; Zuriarrain, J. Detection limit estimator for multivariate calibration by an extension of the IUPAC recommendations for univariate methods. *Analyst* **2008**, *133*, 532−539.

https://doi.org/10.1021/acsomega.3c03125
ACS Omega 2023, 8, 29468−29474